



Original Paper

Stress Path Analysis for Characterization of In Situ Stress State and Effect of Reservoir Depletion on Present-Day Stress Magnitudes: Reservoir Geomechanical Modeling in the Gulf of Suez Rift Basin, Egypt

Ahmed Radwan^{1,3} and Souvik Sen^{2,4}

Received 16 May 2020; accepted 4 August 2020
Published online: 20 August 2020

A reservoir geomechanical modeling has been attempted in the hydrocarbon-bearing Miocene formations in the offshore Badri field, Gulf of Suez, Egypt. Pore pressure established from the direct downhole measurements indicated sub-hydrostatic condition in the depleted mid-Miocene Hammam Faraun and Kareem reservoirs. Vertical stress (S_v) estimated using bulk density data yielded an average of 0.98 PSI/feet (22.17 MPa/km) gradient. Magnitudes of minimum (S_{hmin}) and maximum (S_{hmax}) horizontal stresses were deduced from the poro-elastic model. Relative stress magnitudes ($S_v \geq S_{hmax} > S_{hmin}$) reflect a normal faulting tectonic stress in the Badri field. Pore pressure and stress perturbations (ΔPP and ΔS_h) in the depleted reservoirs investigated from actual measurements recognized 'stress path' values of 0.54 and 0.59 against the Hammam Faraun and Kareem Formations, respectively. These stress path values are far away from the normal faulting limit (0.68), indicating induced normal faulting or fault reactivation to be unlikely at the present depletion rate.

KEY WORDS: In situ stress, Pore pressure, Depletion, Stress path, Reservoir geomechanics, Badri field.

INTRODUCTION

Reservoir geomechanics plays a vital role in well drilling, horizontal well placement and completion optimization (Zoback 2007; Ramdhan and Gouly 2011; Baouche et al. 2020a, b). An accurate

assessment of the magnitudes of pore pressure (PP) and principal stresses [vertical stress (S_v) and two horizontal stress tensors—minimum (S_{hmin}) and maximum (S_{hmax}) horizontal stresses] is an important aspect of comprehensive geomechanical modeling (Ganguli 2017; Ganguli et al. 2018; Radwan et al. 2019a, 2020a; Ganguli and Sen 2020), as it helps in understanding the potential risk of production-induced faulting, wellbore instability and solid production (Zoback and Zinke 2002; Haug et al. 2018). Stress state changes in subsurface reservoirs are controlled by changes in PP due to fluid drawdown or fluid injection that affected the horizontal stresses magnitudes during the production or gas storage (Ruistuen et al. 1996; Addis

¹Faculty of Geography and Geology, Institute of Geological Sciences, Jagiellonian University, Gronostajowa 3a, 30-387 Kraków, Poland.

²Geologix Limited, Dynasty Building, Wing A, Level 4, Andheri Kurla Road, Andheri (E), Mumbai, Maharashtra 400059, India.

³Exploration Department, Gulf of Suez Petroleum Company, Cairo, Egypt.

⁴To whom correspondence should be addressed; e-mail: souvikseniitb@gmail.com, radwanae@yahoo.com

1997a, b; Hillis 2001; Altmann et al. 2010; Dahm et al. 2015; Mortazavi and Atapour 2018; Li et al. 2019a, b; Candela et al. 2019). Advancing and evolving production from mature basins leads to critical changes in the stress state and causing reservoir depletion that resulted from fluid draw-down (Hol et al. 2018). In addition, fluid injection is usually used in the secondary recovery to increase hydrocarbon production and maintains the reservoir pressure, as well as gas storage (Paslay 1994; Radwan et al. 2019b, c, d). The previously mentioned activities in sedimentary systems can be called human-induced mechanical effects or anthropogenic activities that need to be paid attention to during oil and gas extraction and gas storage processes globally (Hol et al. 2018). Hence, the consequences of stress state change (or PP–stress coupling), which has been recorded in several basins worldwide, cause surface subsidence, field-scale deformation (e.g., Sand production and casing collapse) and fault reactivation in many basins like Brunei (Breckels and van Eekelen 1982), Texas, USA (e.g., Salz 1977; Whitehead et al. 1987), Canada (Ervine and Bell 1987), North Sea (e.g., Teufel et al. 1991; Wirput and Zoback 2000; Van Geuns and van Thienen-Visser 2017; Hol et al. 2018; Candela et al. 2019), France (Maury et al. 1990), Australia (Ruth et al. 2006) and Germany (Dahm et al. 2015).

This work focuses on reservoir geomechanical modeling in the offshore Badri field, a proven hydrocarbon accumulation in the Gulf of Suez, Egypt. The Middle Miocene Hammam Faraun and Kareem Formations are the two principal hydrocarbon-bearing units in the Badri field (Radwan et al. 2019a, b, 2020a; Radwan 2020c), which are presently in depleted condition due to prolonged production. In this field, there have been no prior published works on the present-day in situ stress distribution and the effect of depletion in stress magnitudes. We took this opportunity to address these geomechanical aspects, the primary goals of this study are to (a) assess the magnitudes of the three principal stress components, (b) interpret the prevailing tectonic stress regime, (c) quantify the drop in PP and S_{hmin} in depleted reservoirs, (d) establish the depletion-induced reservoir stress path and (e) link the stress path value of the studied reservoirs with it is similar globally. Being an old producing oil field, data availability is a major issue that poses challenges in various steps of the geomechanical modeling. However, to overcome this common issue, we have employed the standard

accepted workflows and modeling techniques to quantify the principal stress magnitudes.

GEOLOGICAL SETTINGS

The African plate separated from the Arabian plate during Late Oligocene–Early Miocene (Bosworth and McClay 2001), and because of the continental rifting, the Gulf of Suez opened up (Schutz 1994; Moustafa 2002). It acts as a northwestern continuation of the well-documented Red Sea rifting system (Bosworth 1995; Bosworth and McClay 2001). It is characterized by a complex pattern of N/NNE–S/SSW- and E–W-trending faults (Abdel-Gawad 1970; Colletta et al. 1988; Evans 1988; Lyberis 1988; Patton et al. 1994; 1995; El-Naby et al. 2009; Youssef 2011; Attia et al. 2015; Abudeif et al. 2016a, b; Radwan et al. 2020b, c) (Fig. 1). The studied offshore Badri hydrocarbon field is situated in one of such structures. It covers $\sim 12 \text{ km}^2$, lying between $28^{\circ}24'–28^{\circ}26' \text{ N}$ and $33^{\circ}22'–33^{\circ}47' \text{ E}$ (Fig. 2). A steeply dipping N–S normal fault separates the studied field from its western neighbor El Morgan field (Abudeif et al. 2016b, 2018; Radwan et al. 2020a). Figure 3 represents the regional lithostratigraphic succession of the study area. During the mid-Miocene active rifting phase, clastic sediments were deposited in the Kareem and Hammam Faraun Formations, which are the principal hydrocarbon-bearing reservoirs in the studied field (Radwan et al. 2019a, 2020a). Reservoir facies is characterized by stacked sandstone units associated with thin shales deposited in a fan delta system (Rhine et al. 1988; EGPC 1996; Peijs et al. 2012; Radwan 2018). The structural contour map at the Belayim Formation top is shown in Figure 4. Late Miocene South Gharib anhydrite acted as seal to the underlying clastic reservoirs (Alsharhan and Salah 1995; Alsharhan 2003; Peijs et al. 2012; Radwan 2014, 2020a, b, c; Rohais et al. 2016).

MATERIALS AND METHODS

Four offshore wells were studied in the Badri field, which encountered roughly 7000 feet¹ of the mid-late Miocene Ras Malaab Group of sediments. Wireline geophysical logs were the primary inputs for all the analyses. Log data were processed for

¹ 1 feet = 3.28 m.

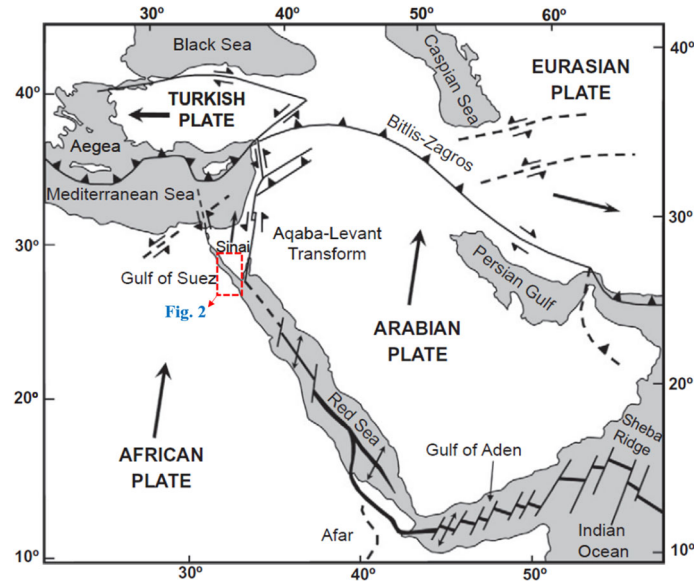


Figure 1. Structural setting of the Gulf of Suez and surrounding areas.

environmental and hole size corrections before utilizing in the analyses. Various downhole measurements, i.e., direct formation pressure and leak-off tests were also available and used for calibration and validation of the estimated parameters. Wireline logs along with the direct downhole measurements have been integrated to estimate the mentioned parameters and ascertain the normal faulting potential in the depleted units. The methods employed in this study are discussed below.

Estimation of Mechanical Properties

Rock strength and elastic properties are the basic inputs to geomechanical modeling. In the absence of core-based static rock property measurements, geophysical logs are employed to estimate these parameters. In this study, the dynamic geomechanical properties were estimated by the following equations (Lal 1999; Chang et al. 2006; Zhang 2013):

$$vd = \frac{Vp^2 - 2Vs^2}{2(Vp^2 - Vs^2)} \quad (1)$$

$$Ed = RHOB \times Vs^2 \left[\frac{3Vp^2 - 4Vs^2}{Vp^2 - Vs^2} \right] \quad (2)$$

$$\mu = \tan \left[\sin^{-1} \left(\frac{Vp - 1000}{Vp + 1000} \right) \right] \quad (3)$$

where *RHOB* indicates log bulk density (gm/cc), *Vp* and *Vs* represent compressional and shear seismic velocities in m/s unit, *d* is log-derived Poisson's ratio (unitless), *Ed* is dynamic Young's modulus (in GPa) unit and μ stands for friction coefficient. Rock strength parameters, i.e., cohesive strength (*c*) and uniaxial compressive strength (*UCS*) were estimated against the reservoir intervals (Hammam Faraun and Kareem Formations) as (Zoback 2007; Khaksar et al. 2009; Zhang et al. 2010):

$$UCS_{Sandstone} = 1200e^{-0.036DT} \quad (4)$$

$$UCS_{Shale} = 1.35 \left(\frac{304.8}{DT} \right)^{2.6} \quad (5)$$

$$c = \frac{UCS \cos \phi}{2(1 - \sin \phi)} \quad (6)$$

where *DT* represents log sonic slowness (is μ s/ft) and generated *UCS* values (in MPa) against sandstones [Eq. (4)] and shales [Eq. (5)], *c* is the cohesion (in MPa) of the rock and ϕ denotes the internal friction angle in degrees.

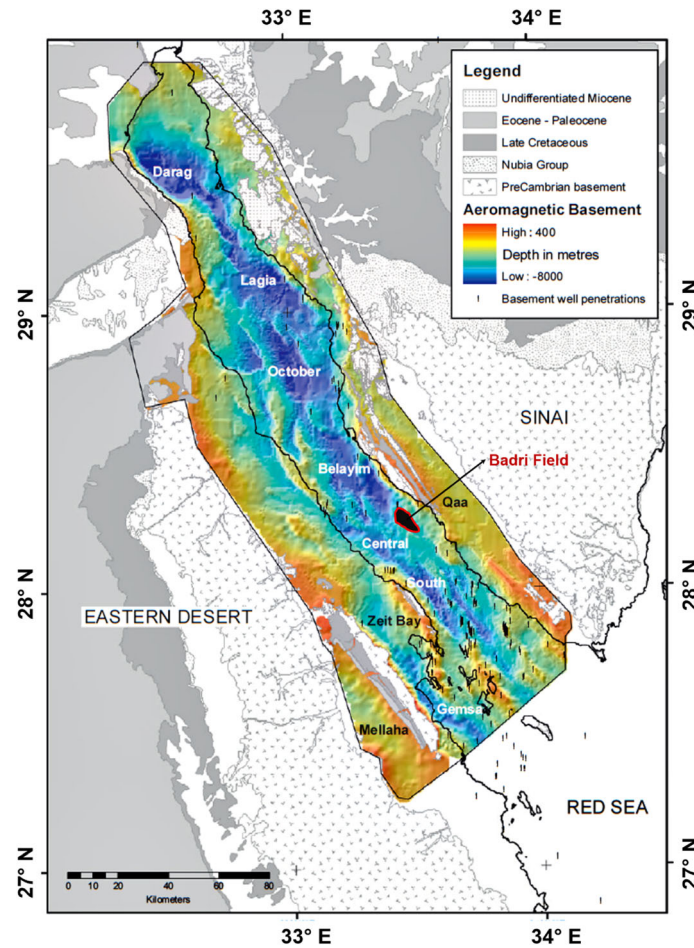


Figure 2. Map of basement depth structure of the Gulf of Suez derived from high-resolution aeromagnetic data (modified from Peijs et al. 2012), showing the location of the studied Badri oil field.

Calculation of S_v Profile

Vertical stress (S_v) at a depth (H) represents the amount of the overburden pressure exerted by a rock column of height H . S_v is calculated using the log density (Plumb et al. 1991):

$$S_v = \int_0^H \text{RHOB}(H) \times g dH \quad (7)$$

where RHOB is log bulk density at the depth (H) of investigation, g is gravitational acceleration (9.8 m/s^2). A continuous density profile is required to estimate a vertical stress profile, but in a practical scenario, wireline density logs are never recorded right from the top of a drilled well leaving a data gap in shallow section (Sen et al. 2017; Ganguli and Sen 2018; Radwan et al. 2019a). Therefore, a synthetic density profile was extrapolated from the surface to

a well's drilled depth/target depth (TD) using the Amoco equation (Sen et al. 2019; Radwan et al. 2019a, 2020a).

Calculation of PP

PP is one of the primary input parameters in geomechanical models, as it affects the magnitudes of horizontal stress components. The most reliable PP estimates come from the direct measurements of downhole formation pressure, but these data are normally acquired against reservoir zones (Ganguli et al. 2017; Sen et al. 2020). There are indirect ways to calculating PP from wireline logs (Zoback 2007; Zhang 2011; Sen et al. 2018a, b; Sen and Ganguli 2019; Baouche et al. 2020c, d) by employing a normal compaction line (NCL). The degree of deviation

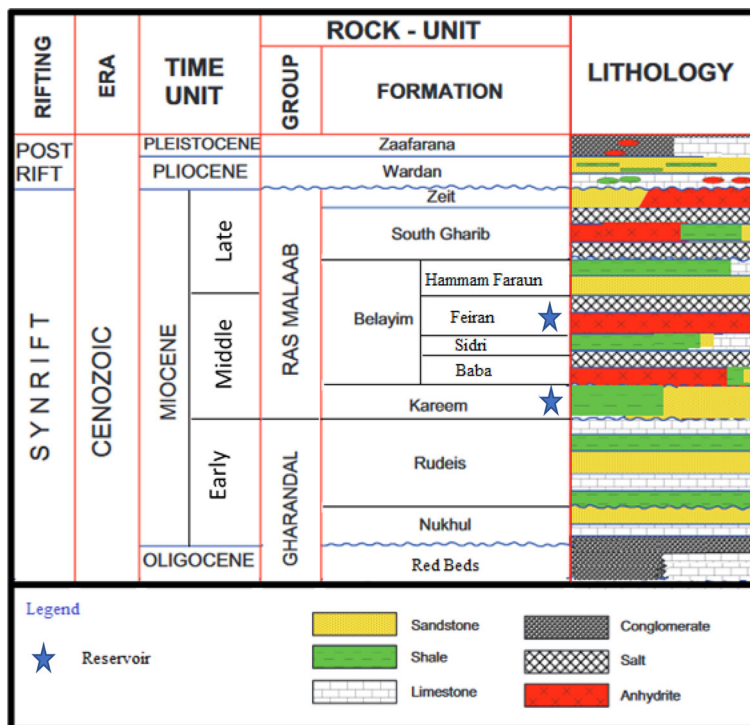


Figure 3. Oligocene recent lithostratigraphy of the Badri oil field (adapted from Radwan 2014, 2018).

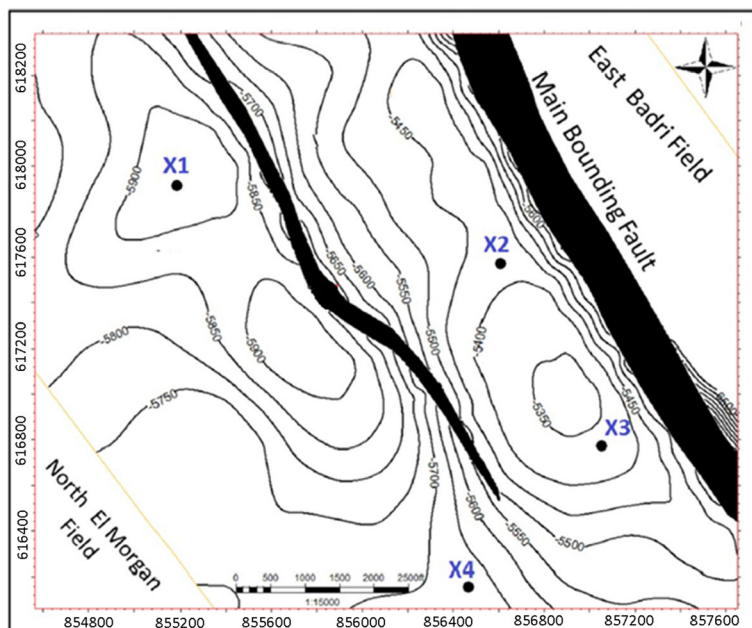


Figure 4. Structural contour map at reservoir top. X1–X4 represent the studied wells in the Badri field. The projection coordinates of the presented map are related to Egypt Gulf of Suez S-650 TL/Red Belt (modified after Abudeif et al. 2018, Radwan et al. 2019a, 2020a, c).

of the mentioned log responses with respect to the NCLs translates to the magnitude of the overpressure (Radwan et al. 2019a, 2020a). However, this method is only applicable to the shale sections. In the studied Badri field, the majority of the lithostratigraphy consists of salt and anhydrites, belonging to Zeit, South Gharib, Feiran and Baba Formations. This possess a huge limitation in employing NCL-based PP estimation method. Therefore, the drilling mud pressure used against these formations was applied as a PP proxy. Usually, mud pressure is kept in such a way that it provides sufficient pressure overbalance (i.e., mud pressure \geq formation PP) to avoid any formation fluid influx. Direct downhole pressure measurements were available against the primary reservoir units, i.e., Hammam Faraun and Kareem Formations, which guided the PP interpretations against these zones.

Calculation of S_{hmin}

In a tectonically active basin, tectonic stresses and strains arise from tectonic plate movement. If tectonic strains are applied to rock formations, these strains add a stress component in an elastic rock. The poro-elastic horizontal strain model considers tectonic strains and therefore accommodates anisotropic horizontal stresses (Blanton and Olson 1999). Because Gulf of Suez is active tectonically, this study employed a poro-elastic horizontal strain model to ascertain S_{hmin} magnitude. This model involves the tectonic strain components (Najibi et al. 2017) acting on two horizontal stress directions (Javani et al. 2017). The S_{hmin} is estimated as:

$$S_{hmin} = \frac{vs}{1 - vs} (Sv - \alpha PP) + \alpha PP + \frac{vEs}{1 - vs^2} (\varepsilon x + vs\varepsilon y) \quad (8)$$

where α denotes the Biot coefficient; and vs and Es denote the static Poisson's ratio and Young's modulus. The Biot coefficient has a default value of 1 (Li et al. 2019a, b; Ganguli and Sen 2020). Laboratory-based rock compressibility and bulk modulus measurements can quantify the Biot coefficient. However, in the absence of core-based measurements, we used the default value for the calculation purpose, which is considered a standard modeling practice (Hofmann et al. 2005; Zoback 2007). Static elastic properties were available from core-based measurements. ' εx ' and ' εy ' indicate the two strain ele-

ments acting on a horizontal plane in mutually perpendicular directions (Kidambi and Kumar 2016; Amiri et al. 2019; Taghipour et al. 2019); thus,

$$\varepsilon x = Sv \frac{vs}{Es} \left(\frac{1}{1 - v} - 1 \right) \quad (9)$$

$$\varepsilon y = Sv \frac{vs}{Es} \left(1 - \frac{v^2}{1 - v} \right) \quad (10)$$

In the absence of core-based elastic property data, empirical relationships by Wang (2000) were used to derive the static elastic properties; thus,

$$vs = vd \quad (11)$$

$$Es = 0.4142 \times Ed - 1.0593 \quad (12)$$

where vs and Es are static Poisson's ratio (unitless) and Young's modulus (in GPa), respectively. Dynamic elastic properties (i.e., vd and Ed) are calculated using Eqs. (1) and (2), respectively. The estimated S_{hmin} was calibrated with formation integrity test (FIT) and leak-off test (LOT) measurements, which are recorded during drilling, usually below the casing setting depths.

Estimation of S_{hmax}

This is the most difficult parameter in geomechanical modeling because there are no direct measurement methods. Wellbore breakout widths (from image logs) are generally used to constrain the S_{hmax} magnitude (Zoback 2007). Zhang (2011) discussed using an empirical tectonic factor (tf) to estimate S_{hmax} , although the output can be vague and largely over-/underestimated if tectonic factor data for the studied area are not well established from a good volume of well data estimates. Since the image log was not run in the studied wells, we used the poro-elastic model to estimate this parameter. Unavailability of image logs is very common in old producing hydrocarbon fields globally, which poses challenges in S_{hmax} magnitude calibration. However, the poro-elastic horizontal strain model is an established S_{hmax} modeling technique in the absence of image log-based calibration data (Kidambi and Kumar 2016; Javani et al. 2017; Najibi et al. 2017; Abbas et al. 2018; Mohammed et al. 2018; Amiri et al. 2019; Taghipour et al. 2019). PP, calibrated with direct measurements, is one of the main input

parameters and, hence, provided increased confidence in this method. The equation is:

$$S_{hmax} = \frac{vS}{1 - vS} (Sv - \alpha PP) + \alpha PP + \frac{ES}{1 - vS^2} (vS\epsilon x + \epsilon y) \quad (13)$$

Input parameters of the above equation are already discussed above.

Stress Path Analysis in a Depleted Reservoir

The stress state within a reservoir is coupled to changes in PP resulting from fluid injection and withdrawal. The most observed coupling is between the least horizontal principal stress and PP. The coupling coefficient, $\Delta S_h/\Delta PP$, is commonly known as the stress path (Santarelli et al. 1998; Gouly 2003). For a reservoir characterized by vertical stresses larger than horizontal stresses, depletion can induce normal faulting when ΔS_h exceeds a critical fraction of ΔPP (Chan and Zoback 2002). The stress path associated with depletion at reservoir scales ranges from 0.34 to 1.18 (Addis1997a; Hillis 2000; Altmann et al. 2010) and it is between 0.6 and 0.8 for overpressured compartments at basin scales (Engelder and Fischer 1994; Hillis 2001; Tingay et al. 2003). Coupling between maximum horizontal principal stress and PP is predicted, but has rarely been reported in the field due to difficulties in measuring the relationship (Zoback and Zinke 2002). Overburden and shear stresses are generally assumed to be decoupled from changes in PP. Based on the poro-elastic theory, the stress path (A) can be expressed mathematically as (Segall and Fitzgerald 1996):

$$A = \frac{\Delta S_h}{\Delta PP} = \alpha \left(\frac{1 - 2v}{v - 1} \right) \quad (14)$$

where α denotes the Biot coefficient. Deformation analysis in reservoir space indicates that, if a depleted reservoir's stress path surpasses a critical value, ΔPP and ΔS_h can induce normal faulting in the reservoir (Zoback and Zinke 2002). In case of a normal faulting scenario, this can be expressed as:

$$\frac{S_v - (PP - \Delta PP)}{(S_h - \Delta S_h) - (PP - \Delta PP)} = \left[\sqrt{\mu^2 + 1} + \mu \right]^2 \quad (15)$$

In terms of stress path, the above equation can be reduced to:

$$A = 1 - \frac{1}{\left[\sqrt{\mu^2 + 1} + \mu \right]^2} \quad (16)$$

Considering $\mu = 0.6$ (Townend and Zoback 2000; Chan and Zoback 2002), the value of A for normal faulting becomes 0.68. The evolution of stress and PP in a depleting producer unit with a steep stress path can induce normal faulting even if the initial stress state is not close to the shear failure (Zoback and Zinke 2002). In case a depleted reservoir attains this A value, the reservoir stress path intersects the normal faulting limit yielding an unstable stress path. Unstable stress path implies the potential for production-induced normal faulting in the depleted reservoir (Chan and Zoback 2002).

RESULTS AND DISCUSSIONS

Downhole pressure measurements were taken by modular dynamic tester tool (MDT) against the two hydrocarbon-bearing formations, which yielded 0.30 and 0.27 PSI/feet PP gradients against the Hammam Faraun and Kareem Formations, respectively, in the present day. We also had access to the reservoir PP measurements taken in the virgin conditions (prior to production). At the in situ pre-production condition, the Hammam Faraun and Kareem Formations exhibited 0.48 and 0.45 PSI/feet gradients, which can be considered hydrostatic. Due to prolonged depletion, both the formations are presently in sub-hydrostatic PP regime. PP in most of the Zeit Formation and the three members (Feiran, Sidri and Baba) of the Belayim Formation have been interpreted as hydrostatic (0.44 PSI/feet). However, because of ductile nature and solubility, salt/halite is hard to drill with hydrostatic mud pressure. Using drilling fluid pressure as PP proxy, an average 0.57–0.60 PSI/feet PP gradient was finalized against the South Gharib Formation and the basal part of the Zeit Formation. The calibrated PP profiles at both present day and virgin conditions are presented in Figure 5. Results indicate that both the hydrocarbon producers (sandstones of the Hammam Faraun and Kareem Formations) are depleted (i.e., they have sub-hydrostatic condition) while hydrostatic pressure condition is retained between non-producer units of the Feiran, Sidri and Baba Formations, indicating an alternating pressure regression profile.

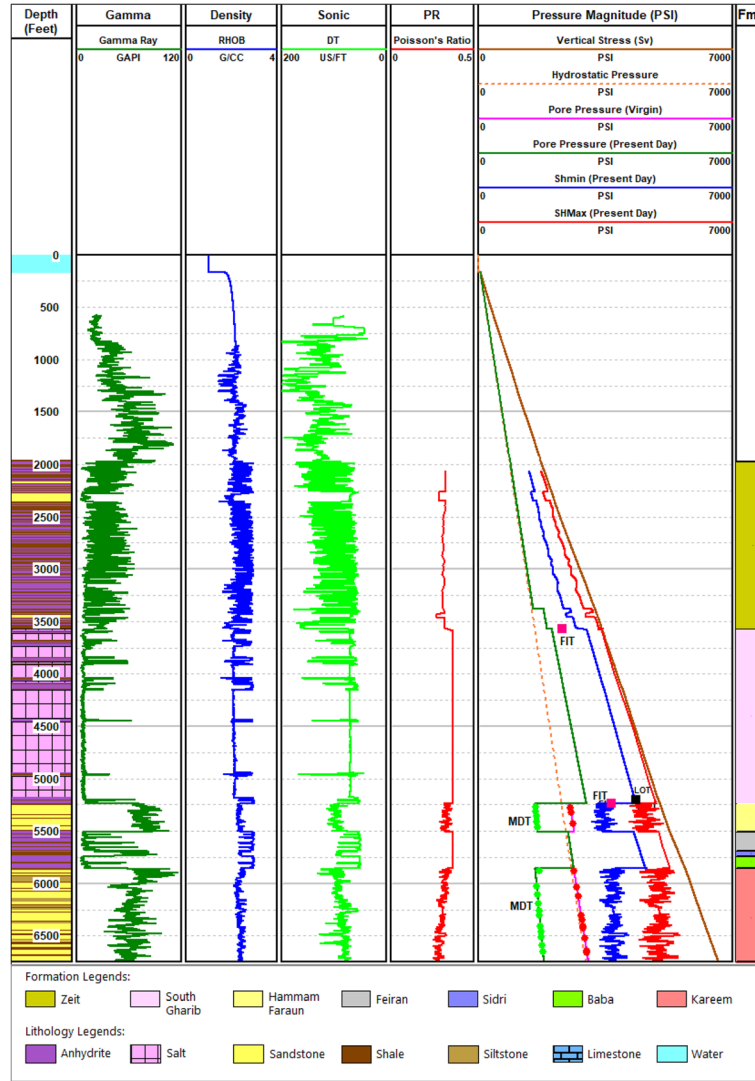


Figure 5. Present-day PP and principal stress magnitudes in well X1, Badri field. ‘MDT’ represents direct measured pore pressure values by Modular Dynamic Tester tool. Green and red dots indicate MDT measurements in depleted and virgin reservoir conditions, respectively. Estimated S_{hmin} is validated with FIT (pink squares) and LOT (black square).

The studied wells have been drilled to average 165–170 feet² of water depth. Extrapolated density profile with a shallowest sediment density of 2.15 g/cc provides the best fitting density trend with the wireline bulk density log (Radwan 2019a, 2020a). Vertical variation of S_v is controlled by lithology. For example, anhydrites possess a higher density (2.9 g/cc) than salt/halite (2.1 g/cc), resulting in higher S_v gradient in the Zeit Formation (0.98 PSI/foot) compared to South Gharib (0.94 PSI/foot). Based on the density log-based estimation, at 7000

feet² TVD (true vertical depth), S_v magnitude is 6850 PSI, which translates to an average 0.978 PSI/foot vertical stress gradient (Fig. 5). Rock mechanical properties were estimated from geophysical logs to characterize formation strength and stiffness, as presented in Figure 6. Based on the log-derived Poisson’s ratio and Young’s modulus and static to dynamic property correlation [Eqs. (11) and (12)], S_{hmin} and S_{hmax} magnitudes were quantified according to the poro-elastic horizontal strain model (Fig. 5). Two FITs and one LOT were available

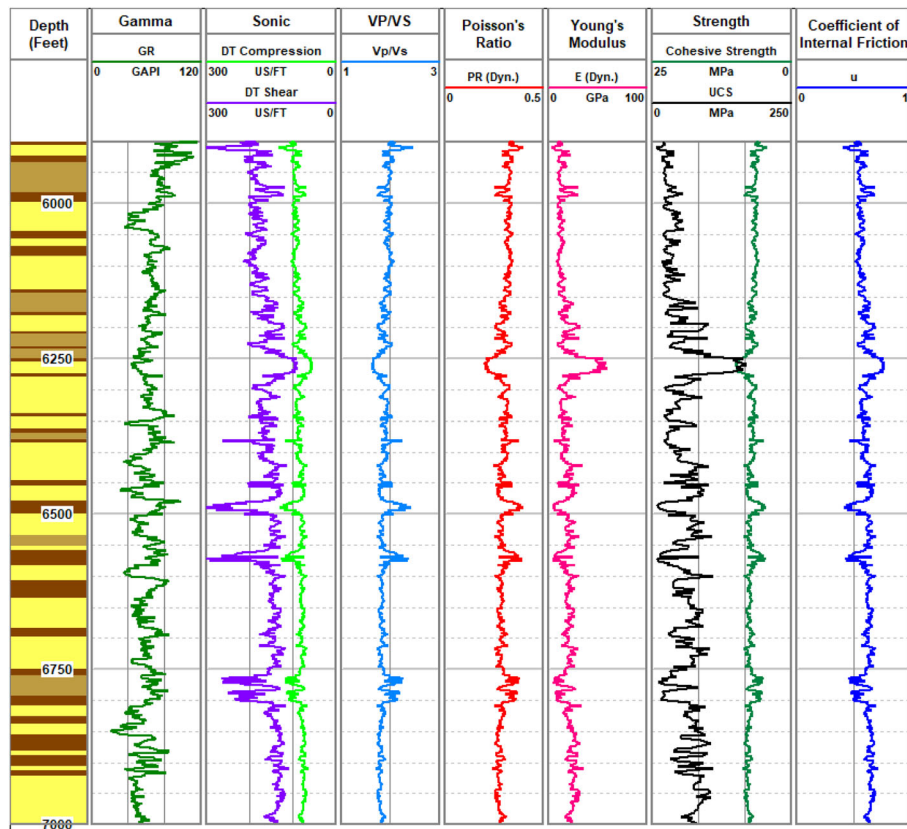


Figure 6. Dynamic elastic parameters (Poisson’s ratio and Young’s modulus), friction coefficient and rock strength (cohesive strength and UCS) estimated from geophysical logs in well X1. The presented interval belongs to the Kareem reservoir unit.

from the lower part of the Zeit and South Gharib Formations, which have been instrumental in the S_{hmin} calibration. Estimated magnitudes (PSI unit³) and gradients (PSI/feet) of PP and principal stress elements are presented in Table 1.

The estimated stress magnitudes indicate that S_v is the highest principal stress and S_{hmin} is the least stress component (Table 1). Based on the relative stress magnitude distributions ($S_v \geq S_{hmax} > S_{hmin}$), a normal faulting stress state is inferred from the studied Badri field. Figure 7 presents a cross-plot between S_v normalized horizontal stress components. Similar stress field observation has been made by Hussein et al. (2013), who interpreted a pure extensional normal faulting regime in the northern (using 18 earthquake events) and southern Gulf of Suez zone (total 79 events) based on the inversion of earthquake focal mechanism (Hussein et al. 2013). Bosworth and Durocher (2017) studied 17 earthquake events ($M \geq 3$) during the last 45 years from the central sub-basin of the Gulf of Suez and inter-

preted a NE–SW extension; the same is supported by wellbore breakout-based observations (Bosworth and Durocher 2017). Zaky (2017) studied the outcrops from the El Quseir region and observed that the Miocene–Pleistocene syn-rift rocks are dissected by a large number of NNW–WNW-oriented normal faults, some of which have oblique slickensides indicating reactivation of these normal faults during a recent extensional movement (Zaky 2017). Our poro-elastic horizontal strain model results are compatible with these previous stress field interpretations, referring to the present-day normal faulting tectonic regime in the studied field.

Based on MDT measurements in depleted and virgin reservoir conditions, PP drop (ΔPP) across the two reservoirs was quantified. Results indicate a 950–1000 PSI² PP reduction in the Hammam Faraun Formation, whereas PP dropped 1070–1200 PSI against the Kareem (Fig. 8). The vertically stacked

² 1 PSI/feet = 22.62 MPa/km; 1 Feet = 3.28 m; 1 PSI = 0.00689 MPa.

Table 1. Estimated magnitudes and gradients of present-day PP and principal stress components

Depth (feet ^a)	Formation	S_v		S_{hmin}		S_{hmax}		PP		Comments
		Magnitude PSI ^b	Gradient PSI/feet ^c	Magnitude PSI ^b	Gradient PSI/feet ^c	Magnitude PSI ^b	Gradient PSI/feet ^c	Magnitude PSI ^b	Gradient PSI/feet ^c	
2100	Zeit	1873	0.89	1443	0.69	1740	0.83	950	0.45	FIT at base 0.65 PSI/feet ^c
2500		2250	0.90	1692	0.68	2086	0.83	1131	0.45	
3000		2815	0.94	2080	0.69	2500	0.83	1357	0.45	
3575		3425	0.96	2600	0.73	3050	0.85	2045	0.57	
3600		3400	0.94	3023	0.84	3300	0.92	2060	0.57	LOT at base 0.84 PSI/feet
4000	Gharib	3800	0.95	3359	0.84	3680	0.92	2300	0.58	
4500		4290	0.95	3773	0.84	4150	0.92	2600	0.58	
5240	Hammam Faraun	5000	0.95	4400	0.84	4800	0.92	3144	0.60	Depleted reservoir, Virgin PP 0.48 PSI/feet ^c
5300		5089	0.96	3400	0.64	4500	0.85	1597	0.30	
5400		5189	0.96	3450	0.64	4535	0.84	1628	0.30	
5500		5291	0.96	3520	0.64	4620	0.84	1658	0.30	
5600	Feiran	5415	0.97	4390	0.78	4985	0.89	2533	0.45	Anhydrite
5680		5513	0.97	4465	0.79	5055	0.89	2569	0.45	
5700	Sidri	5536	0.97	4483	0.79	5073	0.89	2578	0.45	Shale
5735		5572	0.97	4512	0.79	5105	0.89	2594	0.45	
5800	Baba	5655	0.98	4574	0.79	5165	0.89	2623	0.45	Anhydrite
5850		5716	0.98	4620	0.79	5205	0.89	2646	0.45	
5900	Kareem	5769	0.98	3700	0.63	4910	0.83	1595	0.27	Depleted reservoir, Virgin PP 0.45 PSI/feet ^c
6000		5871	0.98	3866	0.64	5001	0.83	1622	0.27	
6500		6379	0.98	4150	0.64	5400	0.83	1757	0.27	
6800		6690	0.98	4380	0.64	5565	0.82	1835	0.27	

^a1 Feet = 3.28 m, ^b1 PSI = 0.00689 MPa, ^cPSI/feet = 22.62 MPa/km

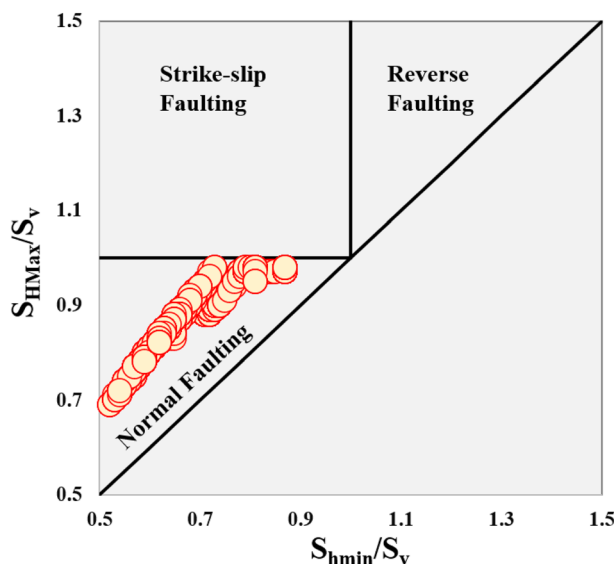


Figure 7. S_v normalized horizontal stress cross-plot from the Badri oil field. Data points indicate a present-day normal fault tectonic stress state in the study area.

Kareem reservoir sandstone units are separated by thin shales over a cumulative 1000 feet¹ vertical thickness. A wide range of ΔPP in the Kareem For-

mation (as interpreted from MDT points) might be due to unequal drawdown from various permeability units across shale barriers. Based on the ΔPP , S_{hmin}

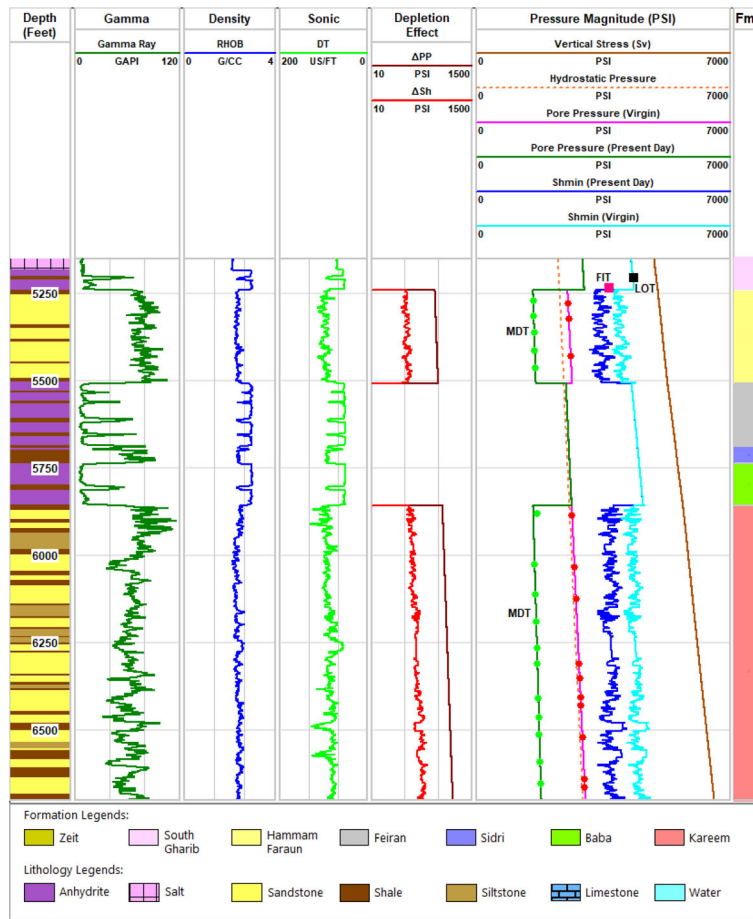


Figure 8. Changes in pore pressure (ΔPP) and minimum horizontal stress (ΔS_h) due to depletion in Track 5. PP and S_h of virgin and depleted conditions are plotted on Track 6, along with the geophysical log signatures and downhole measurements (formation MDT pressure points before and after production, FIT and LOT).

dropped in the range of 500–560 PSI in the Hammam Faraun Formation and 570–790 PSI in the Kareem Formation (Fig. 8). These yielded the average stress path (A) values of 0.54 and 0.59 in the upper and lower reservoirs, respectively. Both estimated A values are still far from the critical failure/faulting limit ($A = 0.68$) (Fig. 9). A higher depletion rate would have potentially increased the stress path values of the reservoirs to the critical level, resulting in depletion-induced reservoir instability. Therefore, it was concluded that the present rate of depletion in the mid-Miocene reservoirs of the Badri oil field will most probably not induce normal faulting.

In this work, we have compared our data with other depleted reservoirs worldwide data to figure out how our findings in the Badri field are far or similar to those in other regions. From our review of

the previously published data by many authors worldwide at reservoir scale (e.g., Salz 1977; Breckels and van Eekelen 1982; Whitehead et al. 1987; Woodland and Bell 1989; Teufel et al. 1991; Addis 1997a, b Hillis 2000; Altmann et al. 2010), we concluded that the least recorded stress path value was 0.34 in Canada, while the highest value was 1.18 and it was recorded in the North Sea (Table 2). Hence, by using a simple approach, we classified the A values into three categories (i.e., high, medium and low). To get the values for each category, we subtracted the lowest and highest values and then divided the result by three to define the boundaries of the proposed three categories. The stress path A values in the low category range from 0.340 to 0.620, in the medium category from 0.621 to 0.900 and in the high category from 0.901 to 1.18. The A values in

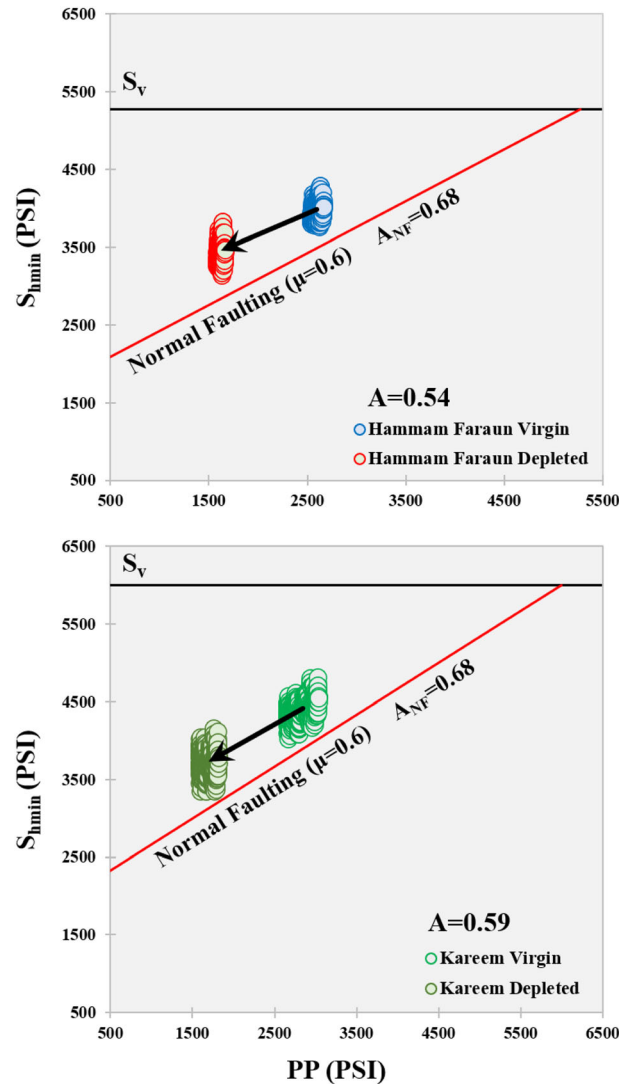


Figure 9. PP- S_h cross-plot and stress path (A) of the Hammam Faraun ($A = 0.54$) and Kareem ($A = 0.59$) Formations along with normal faulting limit. Depletion, in this case, is unlikely to introduce normal faulting in the two reservoirs.

both the middle Miocene reservoirs in this study belong to the low category, similar to Travis Peak Formation and Lake Maracaibo in the USA and Venezuela, respectively (Table 2).

CONCLUSIONS

This study offers a reservoir geomechanical modeling of the Miocene formations in the Badri oil field, offshore Egypt. Pore pressure and three principal stress magnitudes were quantified from geo-

physical logs and calibrated/validated with various downhole measurements. A normal faulting tectonic regime was deciphered in the study area. Reductions in PP and S_{hmin} were inferred in the primary reservoirs, i.e., Hammam Faraun and Kareem Formations, because of prolonged hydrocarbon production. Stress path analysis was performed in both mid-Miocene reservoirs to identify any potential depletion-induced normal faulting. This study will be helpful in future planning of infill well drilling, production rate optimization without inducing any reservoir damage or instability.

Table 2. Stress path values in different depleted reservoirs worldwide including the studied reservoirs

Country/region	Field/basin/formation	Stress Path (A)	Reservoir status	Category	Source
North Sea	West Sole	1.18	Depleted	High (0.901–1.18)	Addis (1997a, b)
North Sea	Ekofisk	0.8	Depleted	Medium (0.621–0.9)	Teufel et al. (1991)
North Sea	Magnus	0.68	Depleted	Medium (0.621–0.9)	Addis (1997a, b)
UK	Wyth Farm	0.65	Depleted	Medium (0.621–0.9)	Addis (1997a, b)
East Texas, USA	Travis Peak Formation	0.57	Depleted	Low (0.34–0.62)	Whitehead et al. (1987)
Venezuela	Lake Maracaibo	0.56	Depleted	Low (0.34–0.62)	Breckels and van Eekelen (1982)
South Texas, USA	Vicksburg Formation	0.48	Depleted	Low (0.34–0.62)	Salz (1977)
Canada	Alberta Basin	0.34	Depleted	Low (0.34–0.62)	Woodland and Bell (1989)
Egypt	Kareem Formation, Badri field, Gulf of Suez Basin	0.59	Depleted	Low (0.34–0.62)	This paper
Egypt	Belayim Formation, Badri field, Gulf of Suez Basin	0.54	Depleted	Low (0.34–0.62)	This paper

ACKNOWLEDGMENTS

We thank Dr. John Carranza, Editor-in-Chief of Natural Resources research, and the two reviewers for their comments and suggestions, which greatly benefited our manuscript. Ahmed Radwan extends his acknowledgment to the ULAM Programme, awarded by the Polish National Agency for Academic Exchange (NAWA) under project PPN/ULM/2019/1/00305/U/00001 for facilitating and funding his research as well as deep thanks to Prof. Alfred Uchman for his continuous support during the research period. Gulf of Suez Petroleum Company (GUPCO) and Egyptian Petroleum Corporation (EPC) are sincerely acknowledged which supported this work with data and required permissions. SS thanks Geologix Limited for providing the access of Pore Pressure and 1D Geomechanics module of GEO Suite of software, which has been instrumental for the analyses presented in this work. Interpretation documented in this manuscript is solely of the authors and does not necessarily represent their respective organizations.

REFERENCES

- Abbas, A. K., Alameedy, U., Alsaba, M., & Rushdi, S. (2018). Wellbore trajectory optimization using rate of penetration and wellbore stability analysis. In *SPE international heavy oil conference and exhibition, Kuwait City, Kuwait, Dec 10-12*. SPE-193755-MS. <https://doi.org/10.2118/193755-ms>.
- Abdel-Gawad, M. (1970). A discussion on the structure and evolution of the Red Sea and the nature of the Red Sea, Gulf of Aden and Ethiopia rift junction—The Gulf of Suez, a brief review of stratigraphy and structure. *Philosophical Transactions of the Royal Society of London. Series A, Mathematical and Physical Sciences*, 267(1181), 41–48.
- Abudeif, A. M., Attia, M. M., Al-Hashab, H. M., & Radwan, A. E. (2018). Hydrocarbon type detection using the synthetic logs: A case study, Baba member, Gulf of Suez, Egypt. *Journal of African Earth Sciences*, 144, 176–182. <https://doi.org/10.1016/j.jafrearsci.2018.04.017>.
- Abudeif, A. M., Attia, M. M., & Radwan, A. E. (2016a). New simulation technique to estimate the hydrocarbon type for the two untested members of Belayim Formation in the absence of pressure data, Badri Field, Gulf of Suez, Egypt. *Arabian Journal of Geosciences*, 9, 218. <https://doi.org/10.1007/s12517-015-2082-2>.
- Abudeif, A. M., Attia, M. M., & Radwan, A. E. (2016b). Petrophysical and petrographic evaluation of Sidri Member of Belayim Formation, Badri field, Gulf of Suez, Egypt. *Journal of African Earth Sciences*, 115, 108–120. <https://doi.org/10.1016/j.jafrearsci.2015.11.028>.
- Addis, M. A. (1997a). Reservoir depletion and its effect on wellbore stability evaluation. *International Journal of Rock Mechanics and Mining Sciences*, 34(3), 4.e1–4.e17.
- Addis, M. A. (1997b). The stress-depletion response of reservoirs. In *SPE annual technical conference and exhibition, San Antonio, TX, Oct 5–8*. <https://doi.org/10.2118/38720-ms>.
- Alsharhan, A. S. (2003). Petroleum geology and potential hydrocarbon plays in the Gulf of Suez rift basin, Egypt. *AAPG Bulletin*, 87(1), 143–180.
- Alsharhan, A. S., & Salah, M. G. (1995). Geology and hydrocarbon habitat in rift setting, northern and central Gulf of Suez, Egypt. *Bulletin of Canadian Petroleum Geology*, 43(2), 156–176.
- Altmann, J. B., Muller, T. M., Muller, B. I. R., Tingay, M. R. P., & Heidbach, O. (2010). Poroelastic contribution to the reservoir stress path. *International Journal of Rock Mechanics and Mining Sciences*, 47(7), 1104–1113.

- Amiri, M., Lashkaripour, G. R., Ghabezloo, S., Moghaddas, N. H., & Tajareh, M. H. (2019). Mechanical earth modeling and fault reactivation for CO₂-enhanced oil recovery in Gachsaran oil field, south-west of Iran. *Environmental Earth Sciences*, 78, 112.
- Attia, M., Abudeif, A., & Radwan, A. (2015). Petrophysical analysis and hydrocarbon potentialities of the untested Middle Miocene Sidri and Baba sandstone of Belayim Formation, Badri field, Gulf of Suez, Egypt. *Journal of African Earth Sciences*, 109, 120–130. <https://doi.org/10.1016/j.jafrearsci.2015.05.020>.
- Baouche, R., Sen, S., & Boutaleb, K. (2020a). Present day in-situ stress magnitude and orientation of horizontal stress components in the eastern Illizi basin, Algeria: A geomechanical modeling. *Journal of Structural Geology*, 132, 103975. <http://doi.org/10.1016/j.jsg.2019.103975>.
- Baouche, R., Sen, S., & Boutaleb, K. (2020b). Distribution of pore pressure and fracture pressure gradients in the Paleozoic sediments of Takouzet field, Illizi basin, Algeria. *Journal of African Earth Sciences*, 164, 103778. <https://doi.org/10.1016/j.jafrearsci.2020.103778>.
- Baouche, R., Sen, S., & Ganguli, S. S. (2020d). Pore pressure and in situ stress magnitudes in the Bhiret Hammou hydrocarbon field, Berkine Basin, Algeria. *Journal of African Earth Sciences*, 171, 103945. <https://doi.org/10.1016/j.jafrearsci.2020.103945>.
- Baouche, R., Sen, S., Sadaoui, M., Boutaleb, K., & Ganguli, S. S. (2020c). Characterization of pore pressure, fracture pressure, shear failure and its implications for drilling, wellbore stability and completion design—A case study from the Takouzet field, Illizi Basin, Algeria. *Marine and Petroleum Geology*, 120, 104510. <https://doi.org/10.1016/j.marpetgeo.2020.104510>.
- Blanton, T. L., & Olson, J. E. (1999). Stress magnitudes from logs-effects of tectonic strains and temperature. *SPE Reservoir Evaluation & Engineering*, 2(1), 62–68.
- Bosworth, W. (1995). A high-strain rift model for the southern Gulf of Suez (Egypt). In Lambiasi, J. J. (Ed.), *Hydrocarbon Habitat in Rift Basins*, Special Publications (Vol. 80, pp. 72–102). London: Geological Society.
- Bosworth, W., & Durocher, S. (2017). Present-day stress fields of the Gulf of Suez (Egypt) based on exploratory well data: Non-uniform regional extension and its relation to inherited structures and local plate motion. *Journal of African Earth Sciences*, 136, 136–147.
- Bosworth, W., & McClay, K. R. (2001). Structural and stratigraphic evolution of the Gulf of Suez rift: A synthesis. In P. A. Zeigler, W. Cavazza, A. H. F. R. Robertson, & S. Crasquin Soleau (Eds.), *Periethyan Rift/Wrench basins and passive margins* (Vol. 186, pp. 567–606). Memoirs: Museum National d'Historie Naturelle de Paris.
- Breckels, I. M., & van Eekelen, H. A. M. (1982). Relationship between horizontal stress and depth in sedimentary basins. *Journal of Petroleum Technology*, 34(09), 2191–2199. <http://doi.org/10.2118/10336-PA>.
- Candela, T., Osinga, S., Ampuero, J., Wassing, B., Pluymaekers, M., Fokker, P. A., et al. (2019). Depletion-induced seismicity at the Groningen gas field, Coulomb rate-and-state models including differential compaction effect. *Journal of Geophysical Research, Solid Earth*, 124(7), 7081–7104.
- Chan, A. W., & Zoback, M. D. (2002). Deformation Analysis in Reservoir Space (DARS): A simple formalism for prediction of reservoir deformation with depletion. In *SPE/ISRM rock mechanics conference, Irving, TX, Oct 20–23*. SPE/ISRM 78174. <https://doi.org/10.2118/78174-ms>.
- Chang, C., Zoback, M. D., & Khaskar, A. (2006). Empirical relations between rock strength and physical properties in sedimentary rocks. *Journal of Petroleum Science and Engineering*, 51, 223–237.
- Colletta, B. P. L. Q., Le Quellec, P., Letouzey, J., & Moretti, I. (1988). Longitudinal evolution of the Suez rift structure (Egypt). *Tectonophysics*, 153(1–4), 221–233.
- Dahm, T., Cesca, S., Hainzl, S., Braun, T., & Krüger, F. (2015). Discrimination between induced, triggered, and natural earthquakes close to hydro-carbon reservoirs: A probabilistic approach based on the modeling of depletion-induced stress changes and seismological source parameters. *Journal of Geophysical Research Solid Earth*, 120, 2491–2509.
- Egyptian General Petroleum Corporation (EGPC). (1996). *Gulf of Suez oil fields (A comprehensive overview)*.
- El-Naby, A. A., El-Aal, M. A., Kuss, J., Boukhary, M., & Lashin, A. (2009). Structural and basin evolution in Miocene time, southwestern Gulf of Suez, Egypt. *Neues Jahrbuch für Geologie und Paläontologie - Abhandlungen*, 251(3), 331–353. <https://doi.org/10.1127/0077-7749/2009/0251-0331>.
- Engelder, T., & Fischer, M. P. (1994). Influence of poroelastic behavior on the magnitude of minimum horizontal stress, Sh in over pressured parts of sedimentary basins. *Geology*, 22(10), 949–952.
- Ervine, W. B., & Bell, J. S. (1987). Subsurface in situ stress magnitudes from oil-well drilling records, an example from the Venture area, offshore eastern Canada. *Canadian Journal of Earth Sciences*, 24(9), 1748–1759.
- Evans, A. L. (1988). Neogene tectonic and stratigraphic events in the Gulf of Suez rift area, Egypt. *Tectonophysics*, 153(1–4), 235–247.
- Ganguli, S. S. (2017). *Integrated Reservoir Studies for CO₂-enhanced oil recovery and sequestration: Application to an Indian Mature Oil Field*. Springer Thesis Series. Berlin: Springer; ISBN: 978-3-319-55842-4. <https://doi.org/10.1007/978-3-319-55843-1>.
- Ganguli, S. S., & Sen, S. (2018). A comprehensive geomechanical assessment of an Indian mature oil field for CO₂-enhanced oil recovery and its sequestration. In *American Geophysical Union (AGU) fall meeting, Washington, DC, December 10–14*.
- Ganguli, S. S., & Sen, S. (2020). Investigation of present-day in situ stresses and pore pressure in the south Cambay Basin, western India, Implications for drilling, reservoir development and fault reactivation. *Marine and Petroleum Geology*, 118, 104422. <https://doi.org/10.1016/j.marpetgeo.2020.104422>.
- Ganguli, S. S., Sen, S., & Kumar, M. (2017). Geomechanical analysis for feasible CO₂ storage in an Indian mature oil field. In *12th Biennial international conference & exposition, SPG, Jaipur, India November 17–19*.
- Ganguli, S. S., Vedanti, N., Pandey, O. P., & Dimri, V. P. (2018). Deep thermal regime, temperature induced over-pressured zone and implications for hydrocarbon potential in the Ankleshwar oil field, Cambay basin, India. *Journal of Asian Earth Sciences*, 161, 93–102.
- Gouly, N. R. (2003). Reservoir stress path during depletion of Norwegian chalk oilfields. *Petroleum Geoscience*, 9, 233–241.
- Haug, C., Nüchter, J.-A., & Henk, A. (2018). Assessment of geological factors potentially affecting production-induced seismicity in North German gas field. *Geomechanics for Energy and Environment*, 16, 15–31.
- Hillis, R. (2000). Pore pressure/stress coupling and its implications for seismicity. *Exploration Geophysics*, 31(2), 448–454.
- Hillis, R. R. (2001). Coupled changes in pore pressure and stress in oil fields and sedimentary basins. *Petroleum Geoscience*, 7, 419–425.
- Hofmann, R., Xu, X., Batzle, M., Prasad, M., Furre, A. K., & Pillitteri, A. (2005). Effective pressure or what is the effect of pressure? *Lead. Edge*, 24, 1256–1260.
- Hol, S., van der Linden, A., Bierman, S., Marcellis, F., & Makurat, A. (2018). Rock physical controls on production-induced compaction in the Groningen field. *Scientific Reports*, 8, 7156.

- Hussein, H. M., Elenean, K. M., Marzouk, I. A., Korrat, I. M., Abu El-Nader, I. F., Ghazala, H., et al. (2013). Present-day tectonic stress regime in Egypt and surrounding area based on inversion of earthquake focal mechanisms. *Journal of African Earth Sciences*, 81, 1–15.
- Javani, D., Aadnoy, B., Rastegarnia, M., Nadimi, S., Aghighi, M. A., & Maleki, B. (2017). Failure criterion effect on solid production and selection of completion solution. *Journal of Rock Mechanics and Geotechnical Engineering*, 9, 1123–1130.
- Khaksar, A., Taylor, P. G., Fang, Z., Kayes, T., Salazar, A., & Rahman, K. (2009). Rock strength from core and logs, where we stand and ways to go. In *SPE EUROPEC/EAGE annual conference and exhibition held in Amsterdam, the Netherlands, June 8–11*, SPE 121972. <https://doi.org/10.2118/121972-ms>.
- Kidambi, T., & Kumar, G. S. (2016). Mechanical earth modeling for a vertical well drilled in a naturally fractured tight carbonate gas reservoir in the Persian Gulf. *Journal of Petroleum Science and Engineering*, 141, 38–51.
- Knott, S. D., Beach, A., Welbon, A. I., & Brockbank, P. J. (1995). Basin inversion in the Gulf of Suez, implications for exploration and development in failed rifts. *Geological Society, London, Special Publications*, 88(1), 59–81.
- Lal, M. (1999). Shale stability, drilling fluid interaction and shale strength. In *SPE Latin American and Caribbean petroleum engineering conference, Caracas Venezuela, April 21–23*. <https://doi.org/10.2118/54356-ms>.
- Li, Q., Aguilera, R., & Ley, H. C. (2019). A correlation for estimating Biot coefficient. In *SPE Western regional meeting, San Jose, CA, USA, April 23–26*. SPE 195359. <https://doi.org/10.2118/195359-ms>.
- Li, L., Tan, J., Wood, D. A., Zhao, Z., Becker, D., Lyu, Q., et al. (2019b). A review of the current status of induced seismicity monitoring for hydraulic fracturing in unconventional tight oil and gas reservoirs. *Fuel*, 242, 195–210.
- Lyberis, N. (1988). Tectonic evolution of the Gulf of Suez and the Gulf of Aqaba. *Tectonophysics*, 153(1–4), 209–220.
- Maury, V., Grasso, J. R., & Wittlinger, G. (1990). Lacq gas field (France), monitoring of induced subsidence and seismicity consequences on gas production and field operation. In *European petroleum conference, Hague, the Netherlands, Oct 21–24*. SPE-20887-MS. <https://doi.org/10.2118/20887-ms>.
- Mohammed, H. Q., Abbas, A. K., & Dahm, H. H. (2018). Wellbore instability analysis for Nahr Umr Formation in Southern Iraq. In *52nd U.S. rock mechanics/geomechanics symposium, Seattle, WA, June 17–20*. ARMA-2018-916.
- Mortazavi, A., & Atapour, H. (2018). An experimental study of stress changes induced by reservoir depletion under true triaxial stress loading conditions. *Journal of Petroleum Science and Engineering*, 171, 1366–1377.
- Moustafa, A. R. (2002). Controls on the geometry of transfer zones in the Suez rift and northwest Red Sea: Implications for the structural geometry of rift systems. *AAPG Bulletin*, 86, 979–1002.
- Najibi, A. R., Ghafoori, M., Lashkaripour, G. R., & Asef, M. R. (2017). Reservoir geomechanical modeling: In-situ stress, pore pressure, and mud design. *Journal of Petroleum Science and Engineering*, 151, 31–39.
- Pasley, P. R. (1994). Stress analysis of drillstrings. In *University of Tulsa Centennial petroleum engineering symposium*. <https://doi.org/10.2118/27976-ms>.
- Patton, T. L., Moustafa, A. R., Nelson, R. A., & Abdine, S. A. (1994). *Tectonic evolution and structural setting of the Suez Rift, Chapter 1, Part I. Type Basin, Gulf of Suez*.
- Peijs, J. A. M. M., Bevan, T. G., & Piombino, J. T. (2012). The Gulf of Suez rift basin. In D. F. G. Roberts & A. W. Bally (Eds.), *Regional geology and tectonics, Phanerozoic rift systems and sedimentary basins* (pp. 164–194). Amsterdam: Elsevier.
- Plumb, R. A., Evans, K. F., & Engelder, T. (1991). Geophysical log responses and their correlation with bed to bed stress contrasts in Paleozoic rocks, Appalachian plateau, New York. *Journal of Geophysical Research*, 91, 14509–14528. <https://doi.org/10.1029/91JB00896>.
- Radwan, A. E. (2014). *Petrophysical evaluation for Sidri and Baba members within Belayim Formation in the region of Badri field, Gulf of Suez, Egypt*. M.Sc. Thesis. <https://doi.org/10.13140/rg.2.2.22772.09601>.
- Radwan, A. E. (2018). *New petrophysical approach and study of the pore pressure and formation damage in Badri, Morgan and Sidki fields, Gulf of Suez Region Egypt*. PhD Thesis. <https://doi.org/10.13140/rg.2.2.26651.82727>.
- Radwan, A. E. (2020a). *Wellbore stability analysis and pore pressure study in Badri field using limited data, Gulf of Suez, Egypt*, AAPG/Datapages Search and Discovery Article #20476 (2020). <https://doi.org/10.1306/20476radwan2020>.
- Radwan, A. E. (2020b). *Hydrocarbon type estimation using the synthetic logs: A case study in Baba Member, Gulf of Suez, Egypt*, AAPG/Datapages Search and Discovery Article #20475 (2020). <https://doi.org/10.1306/20475radwan2020>.
- Radwan, A. E. (2020c). *Effect of clay minerals in oil and gas formation damage problems and production decline: A case study, Gulf of Suez, Egypt*, AAPG/Datapages Search and Discovery Article #20477 (2020). <https://doi.org/10.1306/20477radwan2020>.
- Radwan, A. E., Abudeif, A. M., & Attia, M. M. (2020c). Investigative petrophysical fingerprint technique using conventional and synthetic logs in siliciclastic reservoirs: A case study, Gulf of Suez basin, Egypt. *Journal of African Earth Sciences*, 167, 103868. <https://doi.org/10.1016/j.jafrearsci.2020.103868>.
- Radwan, A. E., Abudeif, A. M., Attia, M. M., Elkhawaga, M. A., Abdelghany, W. K., & Kasem, A. A. (2020a). Geopressure evaluation using integrated basin modelling, well-logging and reservoir data analysis in the northern part of the Badri oil field, Gulf of Suez, Egypt. *Journal of African Earth Sciences*, 162, 103743. <https://doi.org/10.1016/j.jafrearsci.2019.103743>.
- Radwan, A. E., Abudeif, A. M., Attia, M. M., & Mahmoud, M. (2019a). Development of formation damage diagnosis workflow, application on Hammam Faraun reservoir, a case study, Gulf of Suez, Egypt. *Journal of African Earth Sciences*, 153, 42–53. <https://doi.org/10.1016/j.jafrearsci.2019.02.012>.
- Radwan, A. E., Abudeif, A., Attia, M., & Mahmoud, M. (2019c). Formation damage diagnosis, application on Hammam Faraun Reservoir: A case study. Gulf of Suez, Egypt. In *Offshore Mediterranean conference*. <https://doi.org/10.13140/rg.2.2.22352.66569>.
- Radwan, A. E., Abudeif, A., Attia, M., & Mahmoud, M. (2019d). Development of formation damage diagnosis workflow, application on Hammam Faraun reservoir: A case study, Gulf of Suez, Egypt. In *Offshore Mediterranean conference*. ISBN: 9788894043679-2019.
- Radwan, A. E., Abudeif, A. M., Attia, M. M., & Mohammed, M. A. (2019b). Pore and fracture pressure modeling using direct and indirect methods in Badri Field, Gulf of Suez, Egypt. *Journal of African Earth Sciences*, 156, 133–143. <https://doi.org/10.1016/j.jafrearsci.2019.04.015>.
- Radwan, A. E., Kassem, A. A., & Kassem, A. (2020b). Radwany Formation, a new formation name for the Early-Middle Eocene carbonate sediments of the offshore October oil field, Gulf of Suez, Contribution to the Eocene sediments in Egypt. *Marine and Petroleum Geology*, 116, 104304. <https://doi.org/10.1016/j.marpetgeo.2020.104304>.
- Ramadhan, A. M., & Gouly, N. R. (2011). Overpressure and mudrock compaction in the Lower Kutai Basin, Indonesia, a radical reappraisal. *AAPG Bulletin*, 95, 1725–1744.
- Rhine, J. M., Hassouba, A. B., Shishkevich, L., Shafi, A., Azzazi, G., Nashaat, H., et al. (1988). Evolution of a Miocene fan

- delta, a giant oil field in the Gulf of Suez, Egypt. In *Fan deltas, sedimentology and tectonic settings* (pp. 239–250). London: Blackie and Sons.
- Rohais, S., Barrois, A., Colletta, B., & Moretti, I. (2016). Pre-salt to salt stratigraphic architecture in a rift basin, insights from a basin-scale study of the Gulf of Suez (Egypt). *Arabian Journal of Geosciences*, 9(4), 317.
- Ruistuen, H., Teufel, L. W., & Rhett, D. (1996). Influence of Reservoir stress path on deformation and permeability of weakly cemented sandstone reservoirs. In *SPE annual technical conference and exhibition*. <https://doi.org/10.2118/36535-ms>.
- Ruth, P. J., Nelson, E. J., & Hillis, R. R. (2006). Fault reactivation potential during CO₂ injection in the Gippsland Basin, Australia. *Exploration Geophysics*, 37(1), 50–59.
- Salz, L. B. (1977). Relationship between fracture propagation pressure and pore pressure. In *SPE annual fall technical conference and exhibition*. <https://doi.org/10.2118/6870-ms>.
- Santarelli, F. J., Tronvoll, J. T., Svennekjaer, M., Skeie, H., Henriksen, R., & Bratli, R. K. (1998). Reservoir stress path: The depletion and the rebound. In *SPE/ISRM Eurock, Trondheim, Norway, July 8–10*. SPE/ISRM 47350. <https://doi.org/10.2118/47350-ms>.
- Schutz, K. I. (1994). *Structure and stratigraphy of the Gulf of Suez, Egypt, Chapter 2, Part I*. Type Basin, Gulf of Suez.
- Segall, P., & Fitzgerald, S. D. (1996). A note on induced stress changes in hydrocarbon and geothermal reservoirs. *Tectonophysics*, 289, 117–128.
- Sen, S., Corless, J., Dasgupta, S., Maxwell C., & Kumar, M. (2017). Issues faced while calculating overburden gradient and picking shale zone to predict pore pressure. In *First EAGE workshop on pore pressure prediction, Mar 19–21, Pau, France, Paper Mo PP1B 02*. <https://doi.org/10.3997/2214-4609.201700042>.
- Sen, S., & Ganguli, S. S. (2019). Estimation of pore pressure and fracture gradient in Volve Field, Norwegian North Sea. In *SPE oil and gas India conference and exhibition, Mumbai, India, April 9–11*. SPE-194578-MS. <https://doi.org/10.2118/194578-ms>.
- Sen, S., Kundan, A., Kalpande, V., & Kumar, M. (2019). The present-day state of tectonic stress in the offshore Kutch-Saurashtra Basin, India. *Marine and Petroleum Geology*, 102, 751–758. <https://doi.org/10.1016/j.marpetgeo.2019.01.018>.
- Sen, S., Kundan, A., & Kumar, M. (2018a). Post-drill analysis of pore pressure and fracture gradient from well logs and drilling events—An integrated case study of a high pressure exploratory well from Panna East, Mumbai Offshore basin, India. In *Pore pressure and geomechanics from exploration to abandonment, AAPG Geosciences Technology Workshop, Perth, Australia, June 6–7*. <https://doi.org/10.1306/42289Sen2018>.
- Sen, S., Kundan, A., & Kumar, M. (2020). Modeling pore pressure, fracture pressure and collapse pressure gradients in offshore Panna, Western India, implications for drilling and wellbore stability. *Natural Resources Research*. <https://doi.org/10.1007/s11053-019-09610-5>.
- Sen, S., Maxwell, C., & Kumar, M. (2018b). Real time pore pressure interpretation from drilling events—A case study from high pressure offshore exploratory well. In *Operations geoscience adding value*. London: The Geological Society.
- Taghipour, M., Ghafoori, M., Lashkaripour, G. R., Moghaddas, N. H., & Molaghab, A. (2019). Estimation of the current stress field and fault reactivation analysis in the Asmari reservoir, SW Iran. *Petroleum Science*, 16, 513–526. <https://doi.org/10.1007/s12182-019-0331-9>.
- Teufel L. W., Rhett D. W., & Farrell H. E. (1991). Effect of reservoir depletion and pore pressure drawdown on in situ stress and deformation in the Ekofisk Field, North Sea. *International Journal of Rock Mechanics and Mining Sciences & Geomechanics Abstracts*, 29(2), A101. [https://doi.org/10.1016/0148-9062\(92\)92352-d](https://doi.org/10.1016/0148-9062(92)92352-d).
- Tingay, M. R. P., Hillis, R. R., Morley, C. K., Swarbrick, R. E., & Okpere, E. C. (2003). Pore pressure/stress coupling in Brunei Darussalam—Implications for shale injection. *Geological Society, London, Special Publications*, 216(1), 369–379.
- Townend, J., & Zoback, M. (2000). How faulting keeps the crust strong. *Geology*, 28(5), 399–402. [https://doi.org/10.1130/0091-7613\(2000\)28%3C399:HFKTCS%3E2.0.CO;2](https://doi.org/10.1130/0091-7613(2000)28%3C399:HFKTCS%3E2.0.CO;2).
- Van Geuns, L., & van Thienen-Visser, K. (2017). Editorial. *Netherlands Journal of Geosciences*, 96(5), s1–s2. <https://doi.org/10.1017/njg.2017.39>.
- Wang, H. F. (2000). *Theory of linear poroelasticity*. Princeton: Princeton University Press.
- Whitehead, W. S., Hunt, E. R., & Holditch, S. A. (1987). The effects of lithology and reservoir pressure on the in-situ stresses in the Waskom (Travis Peak) Field. In *SPE/DOE Joint Symposium on Low Permeability Reservoirs, Denver, Colorado, May 18–19*. <https://doi.org/10.2118/16403-ms>.
- Wirput, D. J., & Zoback, M. D. (2000). Abstract, Fault reactivation and hydrocarbon leakage along a previously sealing normal fault in the northern North Sea. *AAPG Bulletin*. <https://doi.org/10.1306/a9673284-1738-11d7-8645000102c1865d>.
- Woodland, D. C., & Bell, J. S. (1989). In situ stress magnitudes from mini-frac records in Western Canada. *Journal of Canadian Petroleum Technology*. <https://doi.org/10.2118/89-05-01>.
- Youssef, A. (2011). Early—Middle Miocene Suez Syn-rift-Basin, Egypt, a sequence stratigraphy framework. *GeoArabia*, 16(1), 113–134.
- Zaky, Kh. S. (2017). Paleostress analysis of the brittle deformations on the Northwestern margin of the Red Sea and the Southern Gulf of Suez, Egypt. *Geotectonics*, 51(6), 625–652.
- Zhang, J. (2011). Pore pressure prediction from well logs, methods, modifications, and new approaches. *Earth-Science Reviews*, 108(1–2), 50–63. <https://doi.org/10.1016/j.earscirev.2011.06.001>.
- Zhang, J. (2013). Borehole stability analysis accounting for anisotropies in drilling to weak bedding planes. *International Journal of Rock Mechanics and Mining Sciences*, 60, 160–170.
- Zhang, L., Cao, P., & Radha, K. C. (2010). Evaluation of rock strength criteria for wellbore stability analysis. *International Journal of Rock Mechanics and Mining Sciences*, 47(8), 1304–1316. <https://doi.org/10.1016/j.ijrmms.2010.09.001>.
- Zoback, M. D. (2007). *Reservoir geomechanics*. CA: Stanford University.
- Zoback, M. D., & Zinke, J. C. (2002). Production-induced normal faulting in the Valhall and Ekofisk oil fields. *Pure and Applied Geophysics*, 159, 403–420.